Fabrication approaches for metallo-dielectric plasmonic waveguides

Maziar P. Nezhad, Steve Zamek, Lin Pang, Yeshaiahu Fainman

University of California, San Diego

ABSTRACT

Different techniques for fabricating long-range plasmonic metallo-dielectric waveguides are discussed. The approaches depend strongly on the material system in use. Specific results are presented for SU8 and PDMS.

Keywords: Plasmonics, long range surface plasmons, SU-8, PDMS, metals, surface adhesion

1- Introduction

Since the first experimental demonstration of long range SPP propagation on metal stripe waveguides in 2000 [1], a variety of photonic devices based on this waveguiding technique have been proposed and demonstrated, most of them being applications that utilize the 1550nm telecommunications wavelengths. This is not surprising, since shorter wavelengths would probably incur to much loss. Among the various examples in this area, we can cite the realization of passive components such as straight waveguides, S-bends, Y-splitters and directional couplers ([2],[3], [4], [5], [6]and [7]), switching devices using thermo-optic ([8] and [2]) and electro-optic ([9]) effects and resonant devices such as Bragg filters and Z-add-drop filters([10] and[11]). Using the Bragg resonators and an external gain element, lasing has been also demonstrated using this technology [12]). A somewhat exotic in-line power meter, operating as a combined bolometer and Wheatstone bridge has also been demonstrated [13].

The main requirement in fabrication of these waveguides is that the refractive index of their upper and lower claddings should be symmetrically matched. Due to the extreme sensitivity of the LRSPP mode to cladding imbalance, it is imperative that the refractive index difference between the upper and lower claddings be less than 0.005. In practice this means that the claddings have to be made of the same material. This places restrictions on the type of material and method of fabrication. For example, using crystalline semiconductors as claddings would pose many problems, since it is not possible to grow a crystalline material on top of the non-ordered metal layer. In this work, polymers were chosen as claddings due to the relative ease that they could be spin coated or flowed to create multiple layers. Specifically we present results for the polymers SU-8 and polydimethylsiloxane (PDMS).

Since the core of these waveguides consists of a nanometer thin layer of metal, one of the main steps is metal deposition. This can be done through a variety of methods, such as thermal evaporation, electron beam deposition and plasma sputtering. During various stages of this work, all three of these techniques were used. Apart from film quality, the most important parameter to consider is the thickness of the metal layer, which has to be controlled with sub nanometer accuracy. The two approaches for doing this were to either use a calibrated crystal oscillator thickness monitor (in case it was available for a particular machine), or to use evaporation time as a measure of deposited metal thickness. (The calibration was done by depositing a thick layer of gold over a measured period of time and then measuring the film thickness with a stylus based profilometer (a Veeco Dektak 150)).

Advanced Fabrication Technologies for Micro/Nano Optics and Photonics,
edited by Thomas J. Suleski, Winston V. Schoenfeld, Jian Jim Wang, Proc. of SPIE
Vol. 6883, 68830S, (2008) · 0277-786X/08/$18 · doi: 10.1117/12.768161

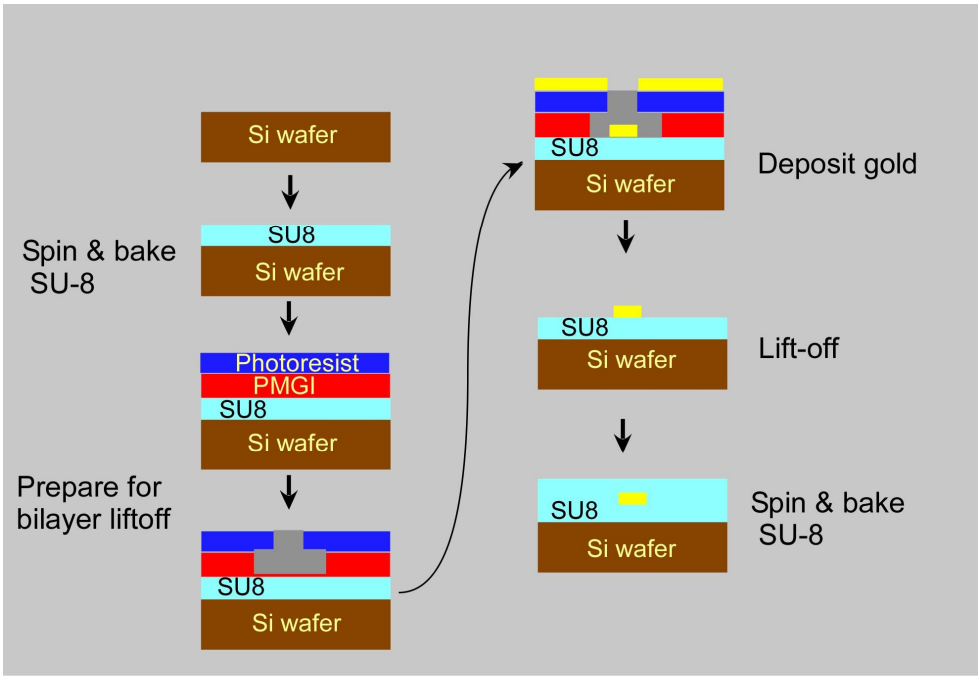

Figure 1. Fabrication steps for creating metal stripe waveguides in SU-8.

2. Fabrication of LRSPP waveguides in SU-8

SU-8 is a chemically amplified epoxy based negative resist with relatively good optical transparency and is sensitive to near UV radiation [14]. Cured films of SU-8 are highly resistant to solvents, acids and bases and have excellent thermal and mechanical stability, making it well suited for permanent use applications. Since SU-8 does not dissolve in any solvent after exposure and bake, it is very easy to spin coat and bake several layers in stacked formation. Also, the higher viscosity solutions can be spun to form layers that are tens of microns thick. Since the cladding around the metal stripe should be thick enough to contain most of the optical mode, this feature of SU-8 is very useful for fabricating LRSPPs.

The fabrication steps are shown in Fig.1. As a first step, a single layer of SU-8 25 was spin coated on top of a silicon wafer at 2000rpm.. The wafer was prepared using ultrasonic cleaning in acetone, and subsequently rinsed with isopropyl alcohol and deionized water and dried for 5 minutes at 200°C. Then a two-step pre-bake was used (3 mins @ 65°C and 7 mins @ 90°C). After pre-baking, the wafer was exposed to UV flood exposure in a Karl Suss MJB3 mask aligner. As a final step, SU-8 requires a post exposure bake to induce crosslinking. This was done in another two- step process (1min @ 65°C and 3mins @ 90°C). At this point the SU-8 had hardened into a 25um thick layer, which comprises the lower cladding.

Since the deposited metal thickness is very small, a liftoff process was used to pattern the metal wires. However, the usual liftoff process involves using a negative resist with negative sloping sidewalls. Getting the profile correct requires tight control over parameters such as exposure dosage and pre- and post- exposure bakes, which can be difficult to maintain on a day to day basis in a shared fabrication facility. Instead, a bilayer liftoff process was used in which a layer of polymethylglutarimide (PMGI SF13 from Microchem) is first spun and baked and then a layer of positive photoresist (Shipley S1805) is spun on top of the PMGI. Since PMGI does not dissolve in most photoresist solvents, no interlayer mixing will happen between it and the S1805.

After exposure of the S1805 (using a patterned quartz photolithography mask and the Karl Suss aligner), the pattern was developed in Shipley MF-321 developer. After the exposed photoresist is dissolved, the developer will start dissolving the underlying PMGI, resulting in a controllable undercut (Fig.2). This undercut makes the liftoff process repeatable and reliable.

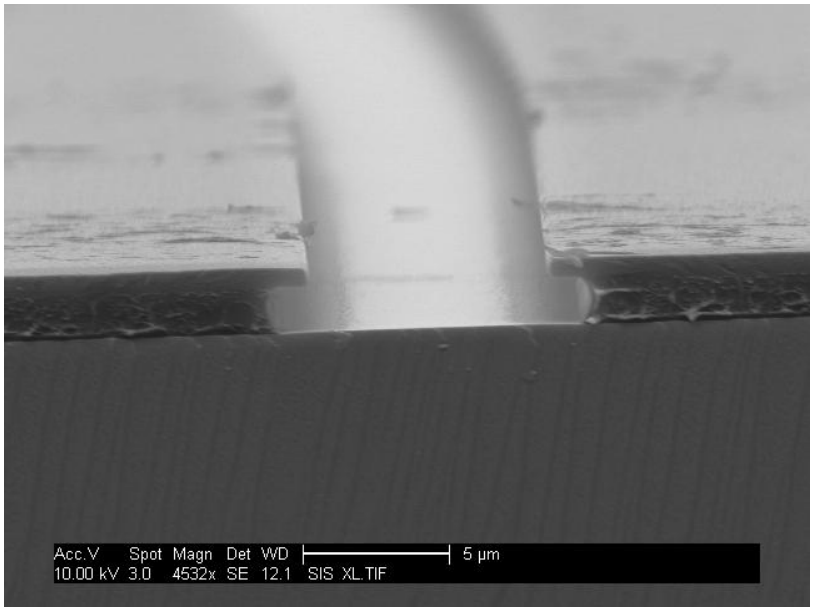

Figure 2. Controllable photoresist undercut using PMGI for metal liftoff. Photoresist is Shipley S1805.

At this point the sample was ready for metal deposition. However, since the adhesion of gold to substrates is notoriously weak, it is common practice to deposit a few nanometers of another metal with better adhesion (e.g., chrome or titanium) in between the gold layer and the substrate. Since the total metal thickness in the LRSPP waveguides is 20nm or less, it was expected that the deposition of an adhesion layer would adversely affect the waveguide characteristics. This is due to two reasons, firstly the symmetry is destroyed and secondly, the chrome layer will add to the metallic losses of the waveguide.

In order to estimate the effects the adhesion layer, a set of finite element simulations were carried out, with gold as the waveguide material and chrome ($\varepsilon = -6.63 + j41.09$ [15]) as the adhesion layer. The gold thickness was kept constant at 20nm and the chrome layer thickness was increased. The results are shown in Fig.3. As seen, the chrome layer has a detrimental effect on the waveguide and increases propagation loss. For example, a 2nm adhesion layer will increase the loss by $2cm^{-1}$ in each of the scenarios mentioned above. Given these results, we decided to refrain from depositing an adhesion layer and carried out liftoff on a directly deposited metal layer, in contradiction to 'conventional' advice. Fortunately, the process worked very well and there was no detachment of the metal waveguides from the SU-8 cladding during the liftoff process. We will revisit this topic at the end of the chapter.

After liftoff, we spun another 25 um layer of SU-8 on top of the metal wires and repeated the bake and exposure steps. At this point, the metal wires are embedded in the SU-8 cladding.

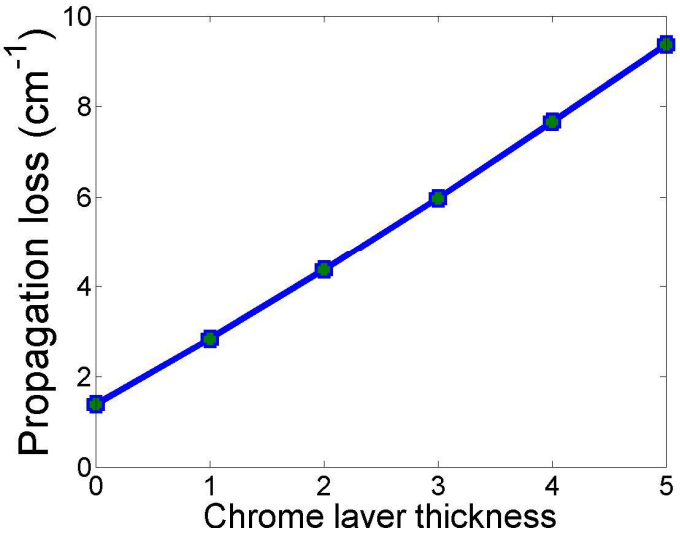

Figure 3. The detrimental effect of a chrome adhesion layer simulated using a finite element mode solver (COMSOL Multiphysics).

2-Fabrication of LRSPP waveguides in polydimethylsiloxane

The previous section described our fabrication approach for SU-8 clad metal waveguides. This approach is fairly general and can be used for other polymers, such as PMMA or BCB [4]. However, this is not the case for the polymer polydimethylsiloxane.

PDMS is a silicon based organic polymer. It has good optical transmission and its hyrophobicity and flow properties have led to its widespread use as a microfluidic and optofluidic fabrication medium (e.g. [16] and [17]). As we mentioned, one of the potential applications of LRSPP waveguides is in optofluidics, so it was a natural step to consider the fabrication of these waveguides in PDMS

One of the characteristics of PDMS is its hydrophobic nature. This feature, while very useful in applications such as microfluidics, poses a problem for lithography, since any attempt to spin coat a photoresist layer will result in the photoresist to fly off the PDMS surface. One way to circumvent this problem is to use an oxygen plasma treatment for activating the surface, which results in a temporary change in the surface chemistry and will allow the photoresist to stick to the PDMS surface, as reported in [18]. This will enable us to pattern the photoresist using a non-contact imaging technique (for example, in [18], the authors create a grating using a two beam interference technique. However, due to the elastic nature of PDMS, any attempt to do a contact lithography step will cause cracks to appear in the baked photoresist (Fig.4.)). Cracks can also appear if the sample is baked at high temperatures, due to the thermal expansion difference between PDMS, silicon and the photoresist. Given these complications, we decided to find other ways of fabricating LRSPP waveguides in PDMS, by making use of the unique features of this elastomer.

Placing embedded metal structures in PDMS has been investigated in the past by different groups, (e.g., [19] and [20]), for the purpose of creating electrodes and other metal structures for lab-on-a-chip, biosensing and electrophoresis applications. One approach, used by Lee *et al.* [19] uses a pattern transfer technique, which seemed to be appropriate for our purposes. In this method, gold patterns are first created on top of a clean silicon substrate, and then treated with an appropriate adhesion agent. This process results in making the gold surface adhesive through the formation of a self assembled monolayer (SAM). Subsequently, uncured PDMS is poured on top of the sample and then cured. The gold patterns will adhere to the PDMS and will be transferred to it after peeling off from the silicon substrate (Fig.5.).

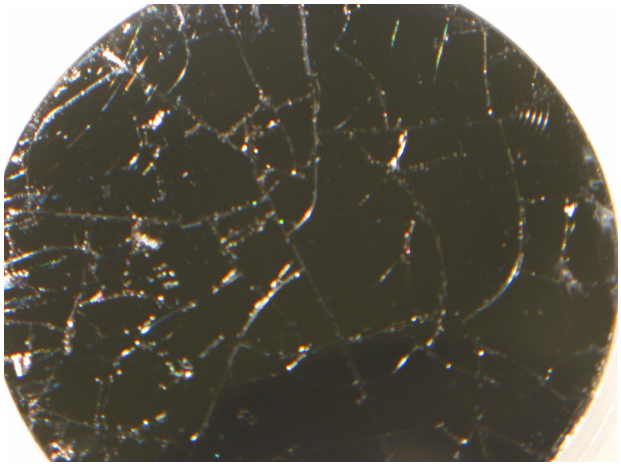

Figure 4. Cracks in S1805 photoresist on a PDMS substrate, spun on top of a silicon wafer.

The cracks happen for two reasons, mechanical stresses applied to to the photoresist layer, due to the elasticity of PDMS and different thermal expansion ratios. Silicon wafers were treated to a sequence of cleaning processes including acetone bath, isopropyl alcohol/deionized water rinse and a Nanostrip® (commercial buffered piranha solution) etch, to ensure their cleanliness. 10 and 20nm thick layers of gold were deposited and patterned using bilayer liftoff. Then the samples were vapor treated with 3-mercaptopropyl trimethoxysilane (MPT from Aldrich) for 40 minutes in vacuum and tridecafluoro-1,1,2,2-tetrahydrooctyl-1-trichlorosilane (TFOS from Gelest Inc.) for 4 minutes at atmospheric pressure. MPT has two types of chain terminators, thiols, which can bond to gold and silane alkoxy terminations, which can bond to PDMS. After the MPT treatment in vacuum a SAM forms on top of the gold layer. The TFOS is a silane release agent, which facilitates the separation of PDMS from the silicon surface. After this treatment, PDMS (standard 10:1 ratio of base:curing agent) was poured over the samples and was cured at 70°C for 40mins.

After the curing process was finished, the PDMS was peeled away from the silicon substrates. However, the results were not satisfactory. The 10nm thick samples did not adhere at all to the PDMS and in the case of the 20nm samples, only the millimeter wide separation borders were transferred in their entirety. Also, some parts of the wider patterns (20□m wide) were transferred to the PDMS. This was unexpected, considering the notoriously weak adhesion of gold to substrates. This led us to carry out a more detailed investigation of the adhesion process, which we will describe in the next section.

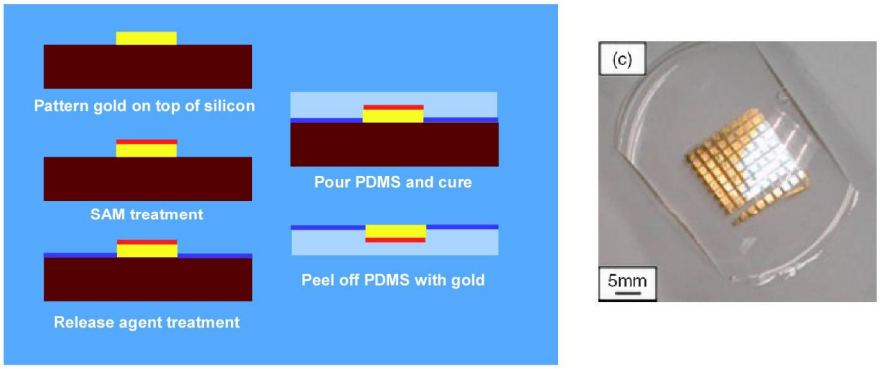

Figure 5. Method of gold pattern transfer to PDMS using self assembled monolayers (SAMs). (from Lee *et al.* [Ref]) .

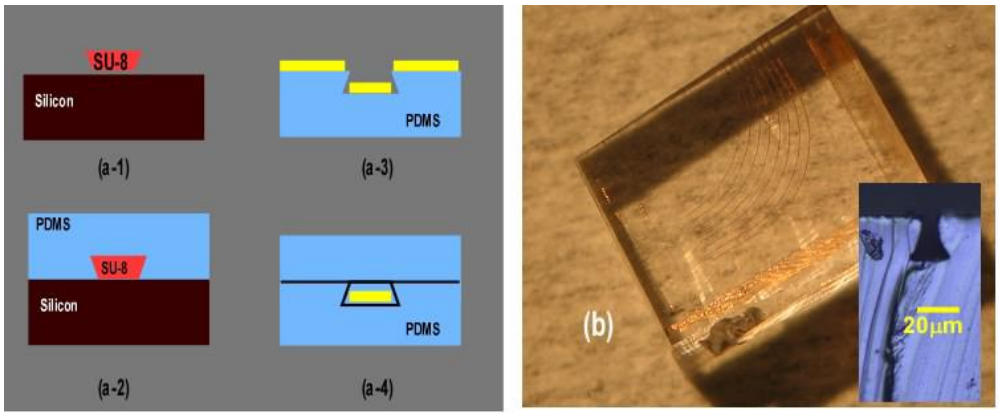

Figure 6. (a) Soft lithography method for creating gold patterns embedded in PDMS. (b) A PDMS sample with 8 micron wide metal wires embedded in it. Inset shows a cross section of PDMS after it was removed from the mold.

Having failed to get the desired results, we decided to try another approach. PDMS has excellent flow properties, which allow it to form microstructures from a master mold. On the other hand, SU-8, being a negative photoresist, can form structures with negative sidewalls, which can then be transferred to PDMS in the molding process. This negative sidewall can be used to create a shading effect during a metal deposition.

Gathering all these properties together, we devised the fabrication approach shown in Fig.6-a. Positive SU-8 patterns were fabricated on a silicon substrate, The sample was treated with a silane release for 4 minutes at atmospheric pressure. Then PDMS was poured over the sample and subsequently was cured (70°C for 1 hour) and peeled off. As seen in inset of Fig.3.11.b, the SU-8 mold leaves an impression with negative slope in the PDMS.

The PDMS sample is then placed inside a deposition chamber and the desired thickness of gold is deposited. As a result, the gold will settle down at the bottom of the trench and on the top surface of the PDMS. At this point, two options present themselves. If the depth of the trench is large enough to isolate the LRSPP mode from the top gold covered surface, we can simply pour uncured PDMS over the sample and cure it. However, the presence of the top metal layer may not be desirable, in which case we add an additional step. Since the adhesion of gold to PDMS is extremely weak, we can easily remove the top layer of gold by applying a sheet of adhesive material (such as Scotch Tape®). This process will not disturb the gold inside the trench. Fig. 6.b shows the final result of this process, with the LRSPP waveguides embedded in PDMS.

3-LRSPP waveguide characterization

To characterize the waveguides, an endfire coupling approach was adopted. The optical setup is shown in Fig.7.a. The laser is operating at 1550nm and the laser output is coupled into a single mode polarization maintaining optical fiber, teminated in either a tapered or a cleaved output. The fiber is positioned on a rotating fiber chuck mounted on a three axis micrometer stage with tip-tilt adjust. Using a free space polarizer, the fiber output was aligned so that the output beam had a vertical polarization.

For imaging the output, a 4-f magnification system was used, with different microscope objectives, ranging from 5x to 40x. The fixed lens had a focal length of 375mm, which resulted in a total magnification of approximately 10-100. For viewing the image, an Indigo Alpha NIR InGaAs camera was used. To examine the polarization of the output, a Glan Thompson polarizer was placed at the camera aperture.

Figs. 7.b and 7.c show the output captured from the smaples clad waveguides, when the polarizer is aligned vertically (TM). In 3.12.b, the fiber is exciting a dielctric mode, but in 3.12.c, the positioning if the fiber is such that it mainly excites the LRSPP mode. By comparing the output to the calculated eigenmode, it is obvious that the spatial properties of the calculated and measured modes are very similar. These are both sufficient evidence that the waveguides are operating as expected. Further optical measurements (such as measuring propagation loss and/or bending loss) are possible and have been well documented by other researchers(e.g., [21], [3] and [5]).

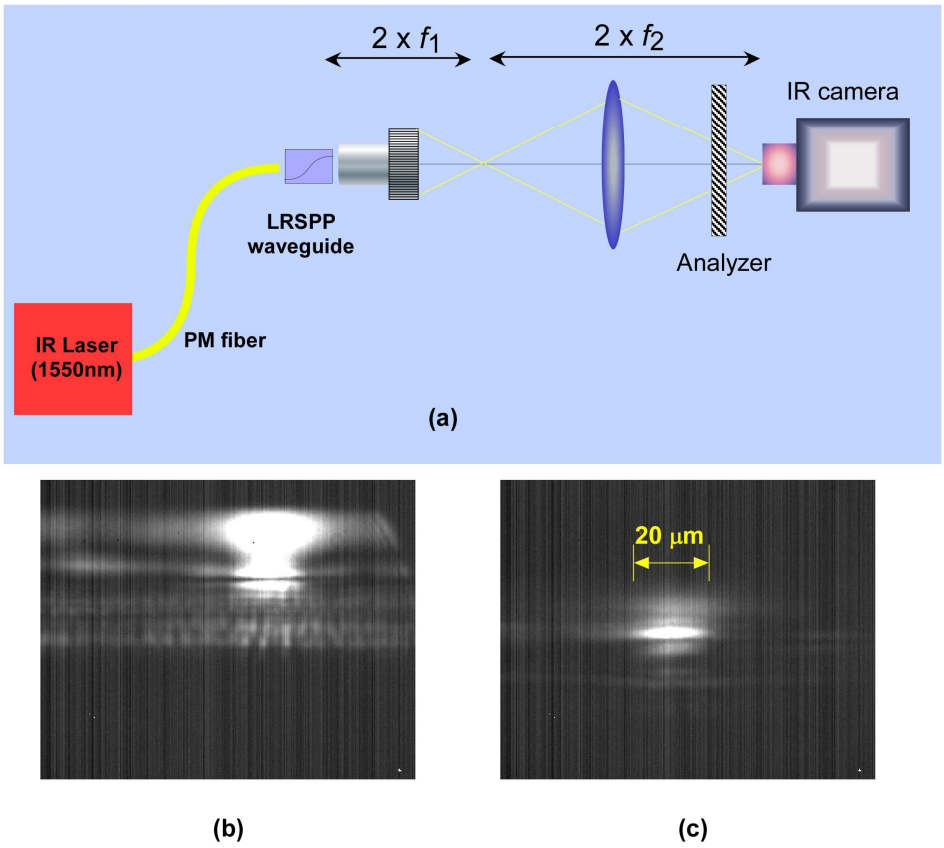

Figure 7. (a) Optical setup for characterizing the LRSPP waveguides. (b) Output of SU-8 clad waveguide when a dielectric slab mode is excited(c) Output of SU-8 clad waveguide with correct end-fire excitation. The mode is a TM mode.

4-Adhesion properties of nanometer thin layers of metals

As we saw in the previous sections, the adhesion properties of our thin gold layers did not seem to follow the generally accepted behavior of such films. Gold is notorious for its weak adhesion and it was therefore surprising to see that our experience with the gold pattern liftoff using PDMS and SAM adhesion promoters [19] was not successful. Also, the plasmonic waveguides on SU-8 seemed to adhere well, without any need for an adhesion layer.

To investigate this in more detail, we carried out a simple experiment. Taking a silicon wafer (which had been thoroughly cleaned by subjecting it to an ultrasonic acetone bath and a Nanostrip treatment), we deposited gold layers of 100nm, 20nm and 10nm thickness using the Denton sputter coater. After that we applied the so-called 'Scotch Tape' test, in which a piece of sticky tape is applied to the surface and then removed. Depending on the quality of adhesion, some or all of the surface film may be removed. In Fig. 8.a we see the result of this test to our three samples. As seen, the 100nm layer of gold is completely removed, while parts of the 20nm film are left on the substrate. Interestingly enough, the 10nm film does not seem to have become detached from the silicon surface.

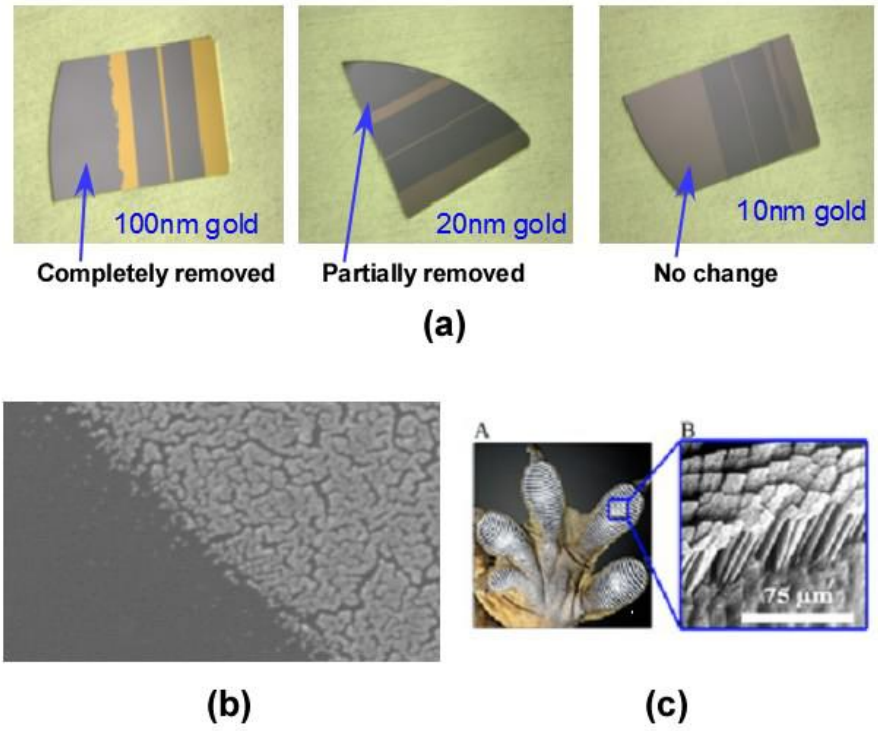

Figure 8. Results of gold adhesion experiment. (a) Different samples showing the success of gold film removal using tape (b) SEM of a nominally 10nm thick gold film. (c) Image of a gecko's foot, showing the microstructured array of setae, which enable it to climb walls.

To find a reason for this phenomenon, we took an SEM image of the 10nm film. As seen in Fig. 8.b, it is still in island form, and a continuous layer has not been formed. It would seem that the minute gold islands have adhesion properties that are quite different from a continuous film.

A reason for this may be the strong Van der Waals forces that exist between nanoparticles. Among other things, this has been suggested as a reason for the adherence of reptile limbs to surfaces, which enables them to climb on vertical structures and has been mimicked artificially under the catchphrase of 'Gecko nanotechnology' [22] .

The net result of this experiment was to provide an explanation for the observed behavior of the nanometer gold films, and remind us that at the nanoscale, things do not always behave as expected.

References

1 R. Charbonneau, P. Berini, E. Berolo, et al., Optics Letters **25**, 844 (2000).
2 T. Nikolajsen, K. Leosson, and S. I. Bozhevolnyi, Applied Physics Letters **85**, 5833 (2004).
3 R. Charbonneau, C. Scales, I. Breukelaar, et al., Journal Of Lightwave Technology **24**, 477 (2006).
4 A. Boltasseva, T. Nikolajsen, K. Leosson, et al., Journal Of Lightwave Technology **23**, 413 (2005).
5 J. T. Kim, S. Park, J. J. Ju, et al., IEEE Photonics Technology Letters **19**, 1374 (2007).
6 J. J. Ju, S. Park, M. S. Kim, et al., Applied Physics Letters **91** (2007).
7 H. S. Won, K. C. Kim, S. H. Song, et al., Applied Physics Letters **88** (2006).
8 T. Nikolajsen, K. Leosson, and S. I. Bozhevolnyi, Optics Communications **244**, 455 (2005).
9 G. Mattiussi, N. Lahoud, R. Charbonneau, et al., Journal Of Vacuum Science & Technology A **25**, 692 (2007).

[10] A. Boltasseva, S. I. Bozhevolnyi, T. Sondergaard, et al., Optics Express **13**, 4237 (2005).
[11] A. Boltasseva, S. I. Bozhevolnyi, T. Nikolajsen, et al., Journal Of Lightwave Technology **24**, 912 (2006).
[12] S. Jetté-Charbonneau and P. Berini, Applied Physics Letters **91**, 181114 (2007).
[13] S. I. Bozhevolnyi, T. Nikolajsen, and K. Leosson, Optics Communications **255**, 51 (2005).
[14] L. Pang, M. Nezhad, U. Levy, et al., Applied Optics **44**, 2377 (2005).
[15] E. D. Palik, *Handbook of Optical Constants of Solids* (Academic Press, 1997).
[16] L. Pang, U. Levy, K. Campbell, et al., Optics Express **13**, 9003 (2005).
[17] K. Campbell, A. Groisman, U. Levy, et al., Applied Physics Letters **85**, 6119 (2004).
[18] V. Lien, Y. Wu, D. Y. Zhang, et al., IEEE Photonics Technology Letters **15**, 712 (2003).
[19] K. J. Lee, K. A. Tosser, and R. G. Nuzzo, Advanced Functional Materials **15**, 557 (2005).
[20] K. S. Lim, W. J. Chang, Y. M. Koo, et al., Lab On A Chip **6**, 578 (2006).
[21] K. Leosson, T. Nikolajsen, A. Boltasseva, et al., Optics Express **14**, 314 (2006).
[22] K. Autumn, American Scientist **94**, 124 (2006).